Mon. Not. R. astr. Soc. (1989) **237,** 355–379

Rapidly rotating general relativistic stars – I. Numerical method and its application to uniformly rotating polytropes

Hidemi Komatsu★ *Department of Astronomy, Faculty of Science, University of Tokyo, Yayoi, Bunkyo-ku, Tokyo 113, Japan*

Yoshiharu Eriguchi *Department of Earth Science and Astronomy, College of Arts and Sciences, University of Tokyo, Komaba, Meguro-ku, Tokyo 153, Japan*

Izumi Hachisu *Department of Physics and Astronomy, Louisiana State University, Baton Rouge, Louisiana 70803-4001, USA, and Department of Aeronautical Engineering, Kyoto University, Yoshida-honmachi, Sakyo-ku, Kyoto 606, Japan*

Accepted 1988 September 13. Received 1988 July 19; in original form 1988 May 9

Summary. We have generalized the Newtonian self-consistent field method to a general relativistic case in order to obtain structures of rapidly rotating relativistic stars. It seems that this method is more powerful than other methods; for any strength of gravity, we can compute equilibrium states if they exist. For the sake of showing the power of this new method, we have computed uniformly rotating polytropic stars having polytropic indices $N=1/2$, $N=3/2$ and $N=3$ for several choices of strength of gravity including the limiting case of strong gravity. Each computed sequence terminates at a critical point where the centrifugal force exactly balances the gravity at the equatorial surface. For strong gravity cases, the configurations of rotating stars look like Newtonian polytropes having much higher polytropic indices, because the mass is concentrated into the central region due to the strong gravity effect. For $N=3/2$ and $N=3$ models, this mass concentration is so large that the critical angular velocity is much smaller than that for Newtonian models having the same polytropic index. As a result, the gravitational mass cannot increase greatly for uniformly rotating configurations.

1 Introduction

Highly relativistic and rapidly rotating objects in an equilibrium configuration have been suggested to exist in quasars, active galactive nuclei and remnants of supernova explosions. However, until recently, they have been little studied in contrast to black holes which are

★Presented as a part of the first author's thesis for the PhD degree to the Department of Astronomy, University of Tokyo.

expressed by analytical generic solutions. Some authors began to compute equilibrium structures of rotating stars numerically. Wilson (1973) computed differentially rotating configurations, and Bonazzola & Schneider (1974) studied rigidly rotating stars by using a self-consistent field (SCF) method. The method is customarily called this after Ostriker & Mark (1968) originated the method to obtain the Newtonian equilibrium states. Their pioneering works in general relativity, however, include some inadequacies in treating the boundary conditions in the asymptotic region. Wilson demonstrated the existence of an ergoregion for rapidly rotating configurations. But his treatment is rather restrictive in the sense that he specified the shape of the density distribution beforehand, and still more he used Newtonian boundary conditions at the boundary of the computational region which might result in inaccuracy for a highly relativistic and highly deformed case. Bonazzola & Schneider showed that in some cases, the equidensity surfaces can become prolate instead of oblate for a degenerate Fermi gas. However it is not clear whether the occurrence of such a configuration is physically real or not. Their method cannot be applied to models having an ergoregion because they used a logarithmic form of the metric tensor, which excludes the possibility of the change of the metric sign. Moreover, although they handled the Einstein equations in an integral form in order that the obtained solutions satisfy the boundary conditions automatically, one of the metric potentials is not guaranteed to satisfy the asymptotic flatness.

Butterworth & Ipser (1975, 1976) treated the Einstein equations in the differential form. They imposed proper boundary conditions derived from an asymptotic expansion and solved Einstein's differential equations directly by using Stoeckly's method (Stoeckly 1965). When the strength of gravity is measured by the ratio of the maximum pressure $p_{\max}$ to the maximum energy density $\varepsilon_{\max}$ at the centre of the star, i.e. $\kappa = p_{\max}/\varepsilon_{\max} c^2$ (see, e.g. Tooper 1964), they succeeded in computing the equilibrium structures up to $\kappa \leq 4.45$ for uniformly rotating homogeneous models. (Strictly speaking, their parameter κ is defined only for spherical configurations.) Although their method was very successful for homogeneous bodies, it did not work for polytropic equations of state when $\kappa > 0.25$ (Butterworth 1976). The reason for this failure has not been clarified yet. After their works, to overcome this difficulty Eriguchi (1980) applied his analytical continuation method (Eriguchi 1978) to uniformly rotating polytropes and succeeded in computing the equilibrium states up to $\kappa \sim 0.5$. Beyond this value of κ, numerical difficulties prevented him from computing highly deformed configurations and he could not obtain critical rotation models at which the gravity at the equatorial surface just balances the centrifugal force there. Recently, using the same numerical scheme as Butterworth & Isper's (1976), Friedman, Isper & Parker (1986) computed uniformly rotating neutron star models for various equations of state proposed for the nuclear density region. Their solutions correspond to models of $\kappa \sim 0.2$. For highly relativistic models having $\kappa \sim 1$, however, no solutions could be obtained except for the homogeneous case even for uniform rotation.

In the present paper, we are going to obtain polytropic models for the case of strong gravity, i.e. up to $\kappa = 1$. In order to handle such strong gravity cases, we need to develop a new powerful method. Very recently, Hachisu (1986a) has proposed a very powerful, brand-new, self-consistent field method for the Newtonian gravity. It seems that this method has no limitations for its applicabilities to various configurations of gaseous bodies and to various equations of state. For example, it enables us to compute ring structures and self-gravitating accretion discs in the two-dimensional axisymmetric case (Hachisu 1986a; Hachisu, Eriguchi & Nomoto 1986a, b) and also to obtain dumb-bell structures and contact phases of a binary in the three-dimensional case (Hachisu 1986b; Hachisu, Eriguchi & Nomoto 1986a, b). Therefore, we adopted this idea to make up our new computational method for general relativity. From now on, we will refer to his method as the HSCF (Hachisu self-consistent field) method.

In this method, the ratio of the polar radius to the equatorial radius, r_p/r_e, is specified to

obtain one model and, further, the equatorial radius of the star is renormalized to be unity. These prescriptions play crucial roles in this numerically stable method. We adopt an integral form of the Einstein equations which is similar to that used by Bonazzola & Schneider (1974) in order for the obtained solutions to satisfy the asymptotic flatness automatically. But, since Bonazzola & Schneider's treatment for one of the metric potentials is improper, as mentioned above, we seek a different way involving the elementary flatness condition on the rotation axis. Utilizing this HSCF method, we can obtain the critical rotation models for the uniformly rotating case up to $\kappa = 1$ and, further, the differentially rotating and self-gravitating tori up to $\kappa \sim 0.2$ or 0.3 for the range of polytropic index $N = 1/2$–$3/2$.

Because the main purpose of this paper is to describe a new numerical scheme for highly relativistic, rapidly rotating configurations, we will show only the results of uniformly rotating stars. The results for differentially rotating stars and for other configurations such as a ring will appear in subsequent papers. In Section 2 assumptions and basic equations are presented. In Section 3 we describe an outline of the numerical method and the detailed technical aspects in our numerical computation. The numerical results are shown in Section 4 for three cases of polytropic indices $N = 1/2$, $N = 3/2$ and $N = 3$, for which solutions are obtained up to the critical rotation.

2 Basic equations and assumptions

2.1 BASIC EQUATIONS

We assume that stars are stationarily rotating and hence have axially, equatorially symmetric structures. The metric can be written in spherical coordinates (t, r, θ, ϕ) as follows:

$$ds^2 = -e^{2\nu}dt^2 + e^{2\alpha}(dr^2 + r^2\,d\theta^2) + e^{2\beta}r^2\sin^2\theta(d\phi - \omega\,dt)^2, \tag{1}$$

where α, β, ν and ω are the potentials which depend only on r and θ. The geometrized units $c = G = 1$ will be used throughout this paper.

The stellar matter is assumed to be a perfect fluid and therefore the energy momentum tensor $\mathbf{T}^{ab}$ is written as:

$$\mathbf{T}^{ab} = (\varepsilon + p)u^a u^b + p\mathbf{g}^{ab}, \tag{2}$$

where ε, p, u^a and $\mathbf{g}^{ab}$ are the energy density, the pressure, the four-velocity and the metric tensor, respectively.

The equation of state obeys a polytropic relation (see, e.g. Tooper 1964; Butterworth 1976), i.e.:

$$p = K\varepsilon^{1+1/N}, \tag{3}$$

where K is a constant and N is the polytropic index.

The Einstein equations for ν, β and ω are written as follows:

$$\Delta[\rho e^{\gamma/2}] = S_\rho(r,\mu), \tag{4}$$

$$\left(\Delta + \frac{1}{r}\frac{\partial}{\partial r} - \frac{1}{r^2}\mu\frac{\partial}{\partial \mu}\right)\gamma e^{\gamma/2} = S_\gamma(r,\mu), \tag{5}$$

$$\left(\Delta + \frac{2}{r}\frac{\partial}{\partial r} - \frac{2}{r^2}\mu\frac{\partial}{\partial \mu}\right)\omega e^{(\gamma-2\rho)/2} = S_\omega(r,\mu), \tag{6}$$

where

$$\Delta=\frac{\partial^2}{\partial r^2}+\frac{2}{r}\frac{\partial}{\partial r}+\frac{1}{r^2}\frac{\partial^2}{\partial\theta^2}+\frac{1}{r^2}\cot\theta\frac{\partial}{\partial\theta}+\frac{1}{r^2\sin^2\theta}\frac{\partial^2}{\partial\phi^2}, \tag{7}$$

$$\gamma=\beta+\nu, \tag{8}$$

$$\rho=\nu-\beta, \tag{9}$$

$$S_\rho(r,\mu)=e^{\gamma/2}\left[8\pi e^{2\alpha}(\varepsilon+p)\frac{1+v^2}{1-v^2}+r^2(1-\mu^2)e^{-2\rho}\left[\omega_{,r}^2+\frac{1}{r^2}(1-\mu^2)\omega_{,\mu}^2\right]\right.$$

$$\left.+\frac{1}{r}\gamma_{,r}-\frac{1}{r^2}\mu\gamma_{,\mu}+\frac{\rho}{2}\left\{16\pi e^{2\alpha}p-\gamma_{,r}\left(\frac{1}{2}\gamma_{,r}+\frac{1}{r}\right)-\frac{1}{r^2}\gamma_{,\mu}\left[\frac{1}{2}\gamma_{,\mu}(1-\mu^2)-\mu\right]\right\}\right], \tag{10}$$

$$S_\gamma(r,\mu)=e^{\gamma/2}\left\{16\pi e^{2\alpha}p+\frac{\gamma}{2}\left[16\pi e^{2\alpha}p-\frac{1}{2}\gamma_{,r}^2-\frac{1}{2r^2}(1-\mu^2)\gamma_{,\mu}^2\right]\right\}, \tag{11}$$

$$S_\omega(r,\mu)=e^{(\gamma-2\rho)/2}\left[-16\pi e^{2\alpha}\frac{(\Omega-\omega)(\varepsilon+p)}{1-v^2}+\omega\left\{-8\pi e^{2\alpha}\frac{[(1+v^2)\varepsilon+2v^2p]}{1-v^2}\right.\right.$$

$$-\frac{1}{r}\left(2\rho_{,r}+\frac{1}{2}\gamma_{,r}\right)+\frac{1}{r^2}\mu\left(2\rho_{,\mu}+\frac{1}{2}\gamma_{,\mu}\right)+\frac{1}{4}(4\rho_{,r}^2-\gamma_{,r}^2) \tag{12}$$

$$\left.\left.+\frac{1}{4r^2}(1-\mu^2)(4\rho_{,\mu}^2-\gamma_{,\mu}^2)-r^2(1-\mu^2)e^{-2\rho}\left[\omega_{,r}^2+\frac{1}{r^2}(1-\mu^2)\omega_{,\mu}^2\right]\right\}\right],$$

from $t-t$, $\phi-\phi$ and $t-\phi$ components of the Ricci tensor, where $\mu=\cos\theta$. In these equations, partial derivatives with respect to r and μ are denoted by $_{,r}$ and $_{,\mu}$, respectively, and v is the proper velocity with respect to the zero angular momentum observer, i.e.:

$$v=(\Omega-\omega)r\sin\theta e^{\beta-\nu}. \tag{13}$$

Here Ω is the angular velocity of the matter measured from infinity. The four-velocity can be expressed as:

$$u^a=\frac{e^{-\nu}}{\sqrt{1-v^2}}(1,0,0,\Omega). \tag{14}$$

The equation of hydrostatic equilibrium is written as:

$$\nabla p+(\varepsilon+p)\left[\nabla\nu+\frac{1}{1-v^2}\left(-v\nabla v+v^2\frac{\nabla\Omega}{\Omega-\omega}\right)\right]=0. \tag{15}$$

In the barotropic case where p depends only on ε, the integrability condition of equation (15) requires that the product of u^t and u_ϕ, i.e. the specific angular momentum measured by the

proper time of matter is a function only of Ω (Bardeen 1970; Butterworth & Isper 1976):

$$u^t u_\phi = \frac{v^2}{(1-v^2)(\Omega-\omega)} = j(\Omega). \tag{16}$$

2.2 ROTATION LAW

We can determine a rotation law by specifying the function $j(\Omega)$. Although this choice of $j(\Omega)$ is arbitrary, stability criteria may impose some constraints on this selection. However, the full precise anlaysis of stability in rapidly rotating relativistic stars has not been studied yet. We will, therefore, choose functional forms based on the results obtained in the Newtonian limit. In the present paper, we consider the simplest selection of $j(\Omega)$ as follows:

$$j(\Omega) = A^2(\Omega_c - \Omega), \tag{17}$$

where A is a positive constant and Ω_c is the angular velocity at the centre of the coordinate system. Here it should be noted Ω_c depends implicitly on the value of A. We will call this A a rotation parameter hereafter. The specific angular momentum $j(\Omega)/u^t$ is related to the metric potentials through equation (16) as:

$$A^2(\Omega_c - \Omega) = \frac{(\Omega-\omega) r^2 \sin^2\theta e^{2(\beta-\nu)}}{1-(\Omega-\omega)^2 r^2 \sin^2\theta e^{2(\beta-\nu)}}. \tag{18}$$

This relation means that the angular velocity on the rotation axis ($\theta = 0$) should be equal to Ω_c.

For the limiting case of large A, $\Omega \to \Omega_c$. Therefore this rotation law approaches a rigid rotation, i.e. the angular velocity Ω is constant in space. For the small value of $A (A \to 0)$, it seems that $\Omega \to \omega$ from equation (18). However this leads to the absurd condition that the dragging potential is equal to the angular velocity even if the gravity is weak. We guess, as $\Omega > \omega$ at some point in space, the right-hand side of equation (18) does not vanish. Thus, the relation:

$$(\Omega_c - \Omega) \sim 1/A^2, \tag{19}$$

must hold as $A \to 0$.

For the Newtonian limit, rotation law (18) can be rewritten as:

$$\Omega/\Omega_c = A^2/(A^2 + \varpi^2), \tag{20}$$

where $\varpi = r\sin\theta$. When $A \to \infty$, it approaches a rigid rotation as mentioned above. When $A \to 0$, it becomes a j-constant rotation, i.e. the specific angular momentum is constant in space (see, e.g. Eriguchi & Müller 1985). This rotation satisfies the Rayleigh criterion for local dynamical stability against axisymmetric disturbances, that is, j should not decrease outward.

2.3 INTEGRAL REPRESENTATION OF BASIC EQUATIONS

In this subsection, we transform the differential form of basic equations into an integral representation. This enables us to handle the boundary conditions (see below) in a much easier manner.

Equation (4) is converted to an integral equation by using a three-dimensional Green's function as follows:

$$\rho = -\frac{1}{4\pi} e^{-\gamma/2} \int_0^\infty dr' \int_{-1}^{1} d\mu' \int_0^{2\pi} d\phi' r'^2 S_\rho(r', \mu') \frac{1}{|\mathbf{r}-\mathbf{r}'|}. \tag{21}$$

By introducing cylindrical coordinates

$$\varpi = r\sin\theta, \qquad z = r\cos\theta, \tag{22}$$

equation (5) for γ can be written as (Bonazzola & Schneider 1974):

$$\frac{\partial^2(\varpi\gamma e^{\gamma/2})}{\partial\varpi^2} + \frac{\partial^2(\varpi\gamma e^{\gamma/2})}{\partial z^2} = \varpi S_\gamma(r,\mu). \tag{23}$$

Using a two-dimensional Green's function, we can have an integral representation of equation (23) as follows:

$$r\sin\theta\gamma = \frac{1}{2\pi} e^{-\gamma/2}\int_0^\infty dr'\int_0^{2\pi} d\theta'\, r'^2 \sin\theta' S_\gamma(r',\theta')\log|\mathbf{r}-\mathbf{r}'|, \tag{24}$$

where we analytically continue $S_\gamma(r,\theta)$ to the range $\pi < \theta \le 2\pi$ by defining:

$$S_\gamma(r,\theta) = S_\gamma(r,\theta-\pi). \tag{25}$$

After multiplying equation (6) by $r\sin\theta\cos\phi$, we obtain:

$$\Delta[r\sin\theta\cos\phi\,\omega e^{(\gamma-2\rho)/2}] = r\sin\theta\cos\phi\, S_\omega(r,\theta). \tag{26}$$

An integral equation for this differential equation can be expressed as follows:

$$r\sin\theta\cos\phi\,\omega = -\frac{1}{4\pi} e^{(2\rho-\gamma)/2}\int_0^\infty dr'\int_0^\pi d\theta'\int_0^{2\pi} d\phi'\, r'^3 \sin^2\theta'\cos\phi' S_\omega(r',\theta')\frac{1}{|\mathbf{r}-\mathbf{r}'|}. \tag{27}$$

Using expansion series for the Green's functions, i.e.:

$$\log|\mathbf{r}-\mathbf{r}'| = \frac{1}{2}\log[r^2 + r'^2 - 2rr'\cos(\theta-\theta')]$$

$$= -\sum_{n=1}^{\infty}\frac{1}{n} f_n^1(r,r')(\cos n\theta\cos n\theta' + \sin n\theta\sin n\theta') + g(r,r'), \tag{28}$$

$$\frac{1}{|\mathbf{r}-\mathbf{r}'|} = \sum_{n=0}^{\infty} f_n^2(r,r')\left[P_n(\cos\theta)P_n(\cos\theta') + 2\sum_{m=1}^{n}\frac{(n-m)!}{(n+m)!}P_n^m(\cos\theta)P_n^m(\cos\theta')\cos m(\phi-\phi')\right], \tag{29}$$

where

$$f_n^1(r,r') = \begin{cases}(r'/r)^n, & \text{for } r'/r \le 1,\\ (r/r')^n, & \text{for } r'/r > 1,\end{cases} \tag{30}$$

$$f_n^2(r,r') = \begin{cases}(1/r)(r'/r)^n, & \text{for } r'/r \le 1,\\ (1/r')(r/r')^n, & \text{for } r'/r > 1,\end{cases} \tag{31}$$

and

$$g(r,r') = \begin{cases}\log(r), & \text{for } r'/r \le 1,\\ \log(r'), & \text{for } r'/r > 1,\end{cases} \tag{32}$$

we have:

$$\rho = -\sum_{n=0}^{\infty} e^{-\gamma/2}\int_0^{\infty} dr'\int_0^1 d\mu'\, r'^2 f_{2n}^2(r,r') P_{2n}(\mu) P_{2n}(\mu') S_\rho(r',\mu'), \tag{33}$$

$$r\sin\theta\gamma = -\frac{2}{\pi}\sum_{n=1}^{\infty} e^{-\gamma/2}\int_0^{\infty} dr'\int_0^1 d\mu'\, r'^2 f_{2n-1}^1(r,r')\frac{1}{2n-1}\sin(2n-1)\theta\times\sin(2n-1)\theta' S_\gamma(r',\mu'), \tag{34}$$

$$r\sin\theta\omega = -\sum_{n=1}^{\infty} e^{(2\rho-\gamma)/2}\int_0^{\infty} dr'\int_0^1 d\mu'\, r'^3 \sin\theta' f_{2n-1}^2(r,r')\frac{1}{2n(2n-1)} \times P_{2n-1}^1(\mu) P_{2n-1}^1(\mu') S_\omega(r',\mu'), \tag{35}$$

respectively. Here, P_n is the Legendre polynomial and P_n^m is the associated Legendre function. In equations (33)–(35), the asymptotic flatness conditions, that is, $\rho \sim O(1/r)$, $\gamma \sim O(1/r^2)$, and $\omega \sim O(1/r^3)$ for $r \to \infty$, are satisfied automatically, if the source terms, S_ρ, S_γ and S_ω, are reasonable.

The potential α is determined from other potentials by the following equation (Butterworth & Ipser 1976), i.e.:

$$\begin{aligned}
\alpha_{,\mu} = &-\nu_{,\mu} - \{(1-\mu^2)(1+rB^{-1}B_{,r})^2 + [\mu-(1-\mu^2)B^{-1}B_{,\mu}]^2\}^{-1} \\
&\left[\tfrac{1}{2}B^{-1}\{r^2 B_{,rr} - [(1-\mu^2)B_{,\mu}]_{,\mu} - 2\mu B_{,\mu}\}[-\mu + (1-\mu^2)B^{-1}B_{,\mu}]\right. \\
&+ rB^{-1}B_{,r}[\tfrac{1}{2}\mu + \mu r B^{-1}B_{,r} + \tfrac{1}{2}(1-\mu^2)B^{-1}B_{,\mu}] \\
&+ \tfrac{3}{2}B^{-1}B_{,\mu}[-\mu^2 + \mu(1-\mu^2)B^{-1}B_{,\mu}] - (1-\mu^2)rB^{-1}B_{,\mu r}(1+rB^{-1}B_{,r}) \\
&- \mu r^2 \nu_{,r}^2 - 2(1-\mu^2)r\nu_{,\mu}\nu_{,r} + \mu(1-\mu^2)\nu_{,\mu}^2 - 2(1-\mu^2)r^2 B^{-1}B_{,r} \\
&\times \nu_{,\mu}\nu_{,r} + (1-\mu^2)B^{-1}B_{,\mu}[r^2\nu_{,r}^2 - (1-\mu^2)\nu_{,\mu}^2] + (1-\mu^2)B^2 e^{-4\nu} \\
&\times [\tfrac{1}{4}\mu r^4 \omega_{,r}^2 + \tfrac{1}{2}(1-\mu^2)r^3\omega_{,\mu}\omega_{,r} - \tfrac{1}{4}\mu(1-\mu^2)r^2\omega_{,\mu}^2 + \tfrac{1}{2}(1-\mu^2) \\
&\left.\times r^4 B^{-1}B_{,r}\omega_{,\mu}\omega_{,r} - \tfrac{1}{4}(1-\mu^2)r^2 B^{-1}B_{,\mu}[r^2\omega_{,r}^2 - (1-\mu^2)\omega_{,\mu}^2]\}\right],
\end{aligned} \tag{36}$$

where

$$B = e^{\gamma} = e^{\beta+\nu}. \tag{37}$$

Here we use μ as an independent variable instead of θ to avoid the apparent singularity of $\cot\theta$ at the pole. Because the flatness condition on the rotation axis requires:

$$\alpha = \beta \quad \text{at} \quad \mu = 1, \tag{38}$$

we can integrate equation (36) starting from the pole to the equator. The obtained potential α always satisfies the asymptotic condition, i.e. $\alpha \sim O(1/r)$ for $r \to \infty$, because the other potentials ν, β, γ and ω fulfil their corresponding asymptotic conditions.

When the integrability condition (16) is satisfied, equation of hydrostatic equilibrium (15) can be integrated with the aid of polytropic relation (3) as follows:

$$(1+N)\ln(K\varepsilon^{1/N}+1) + \nu + \tfrac{1}{2}\ln(1-v^2) + \int j(\Omega)\, d\Omega = 0. \tag{39}$$

Since the rotation law is defined by relation (17), the last term of the left-hand side of equation

(39) can be expressed explicitly and we obtain:

$$(1+N)\ln(K\varepsilon^{1/N}+1)+\nu+\tfrac{1}{2}\ln(1-v^2)-\tfrac{1}{2}A^2(\Omega-\Omega_c)^2=C, \tag{40}$$

where C is an integral constant.

3 Method of solution

3.1 OUTLINE OF THE COMPUTATIONAL PROCEDURE

An equilibrium model can be specified by three parameters, i.e. the ratio of the maximum pressure to the maximum energy density κ, the axis ratio r_p/r_e and the rotation parameter A, where r_p and r_e are the polar radius and the equatorial radius, respectively. We adopt the axis ratio instead of the central angular velocity Ω_c because Ω_c is not a good parameter to specify all models on the equilibrium sequence. For example, there are two solutions with a single value of Ω_c for the Maclaurin spheroids (see, e.g. Chandrasekhar 1969) in the Newtonian limit. This means that if we specify a value of Ω_c we can obtain only one model of the two corresponding models but cannot do the other one. The limiting case of small κ corresponds to Newtonian gravity and we will calculate models up to $\kappa=1$, where the dominant energy condition, i.e. $T^{00}\geq|T^{ab}|$ for each a, b, breaks down (Hawking & Ellis 1973, p. 91).

In the remainder of this subsection, we are going to describe the outline of our numerical procedure. At the beginning of the computation, we prepare initial guesses for the metric potentials ν, α, β, and ω, the energy density ε, and the angular velocity Ω. Substituting them into the integrands of equations (33)–(35), we can obtain new values of ν, β, and ω.

The other metric potential α can be obtained by integrating equation (36), starting from the rotation axis and ending at the equator. It should be noted that new values of ν, β and ω are used in this integration. Using newly obtained values of ν, α, β and ω, we calculate a new energy density ε and new angular velocity Ω. This is one cycle of iteration. These newly obtained values of ν, α, β, ω, ε and Ω are used as an improved set of guesses in the next iteration cycle. When the differences of each physical quantity between two successive cycles become sufficiently small, we regard these obtained values as a solution.

During the iteration procedure, three parameters, i.e. the axis ratio r_p/r_e, the strength of gravity κ, and the rotation parameter A, are fixed. Changing the axis ratio r_p/r_e from model to model, we can have a sequence of solutions for the same κ and the same A.

3.2 ESSENCE OF THE HSCF METHOD

One of the essential techniques in the HSCF method is specifying the axis ratio, i.e. r_p/r_e, during the iteration. Here we will consider a more general case including a ring structure. At first we adopt two boundary points P and Q, where point P is the inner edge and point Q is the outer edge of matter as seen in Fig. 1. The terminology 'axis ratio' is used for the ratio of $r_p=r(\mathrm{P})$ to $r_e=r(\mathrm{Q})$. Point P is set on the rotation axis when the matter has a spheroidal topology while point P is on the equator when it has a toroidal topology. In the present paper, however, we will treat only spheroidal configurations because the equilibrium sequences are terminated long before its configuration becomes a ring for the rigidly rotating case. The other important point is to fix the maximum density $\varepsilon_{\max}$ during the iteration procedure. These two techniques are necessary for us to compute an equilibrium in a numerically stable manner.

These conditions are regarded also as boundary conditions for matter. We introduce the specific enthalpy H after Hachisu (1986a) as follows:

$$\ln H\equiv C-\nu-\tfrac{1}{2}\ln(1-v^2)+\tfrac{1}{2}A^2(\Omega-\Omega_c)^2, \tag{41}$$

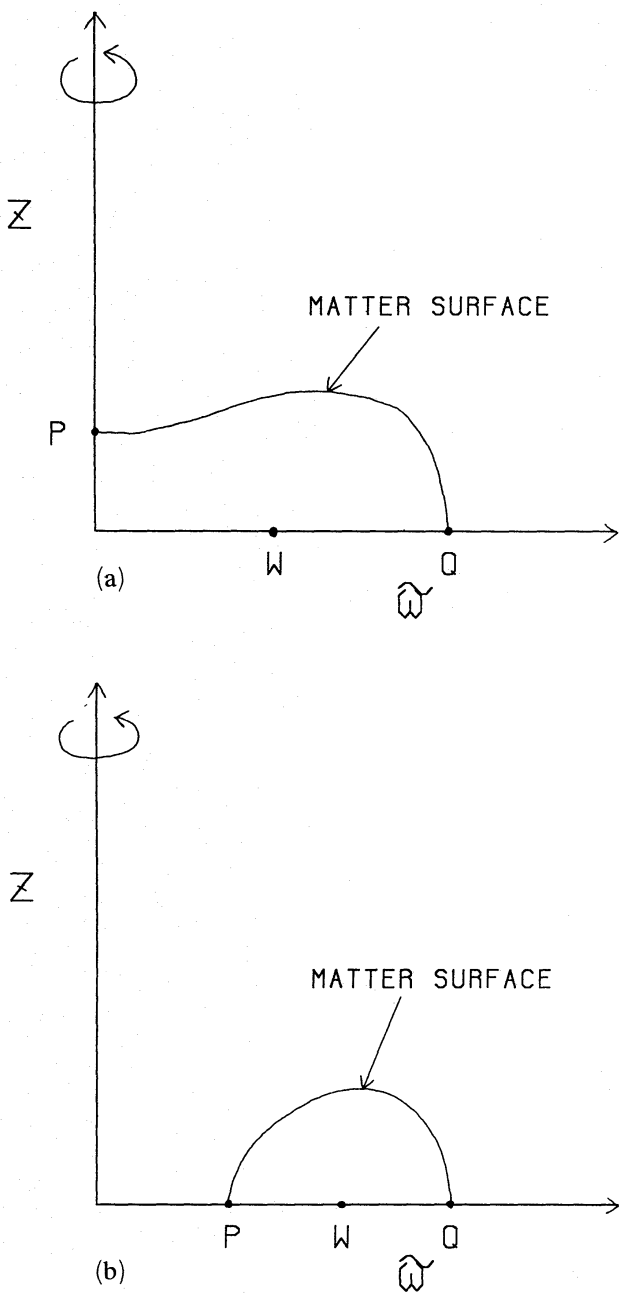

Figure 1. Schematic figures of our computational region. Two edges of matter, i.e. points P and Q, specify a model uniquely. The computational region covers far outside the outer edge of matter. (a) When it is spheroid-like, point P is set on the rotation axis. (b) When it is toroidal, point P is set on the equator. See text for details.

and then the energy density ε is calculated from H as:

$$\varepsilon = [(H^{1/(N+1)} - 1)/K]^N. \tag{42}$$

Since the energy density vanishes at points P and Q, equation (41) becomes:

$$\ln H(\mathrm{P}) = 0, \tag{43}$$

$$\ln H(\mathrm{Q}) = 0. \tag{44}$$

From equation (42), when the energy density attains maximum, the specific enthalpy also

becomes maximum, i.e. $H_{\max}$. This value is related to κ as follows:

$$\ln H_{\max} = (1+N)\ln(\kappa+1), \tag{45}$$

where

$$\kappa = p_{\max}/\varepsilon_{\max} = K\varepsilon_{\max}^{1/N}. \tag{46}$$

Fixing $\varepsilon_{\max}$ is equivalent to fixing κ. So we will use κ instead of $\varepsilon_{\max}$. We denote the point where ε reaches its maximum value by W.

3.3 DETERMINATION OF r_e AND Ω_c

In order to fix points P and Q in our computational space, we introduce a new coordinate system, namely:

$$r = r_e\hat{r}. \tag{47}$$

Then point P is always at $\hat{r}(\mathrm{P}) = r_p/r_e$ and point Q is always at $\hat{r}(\mathrm{Q}) = 1$ in our new computational space. Other physical quantities are transformed as follows:

$$\alpha = r_e^2\hat{\alpha}, \tag{48}$$

$$\beta = r_e^2\hat{\beta}, \tag{49}$$

$$\nu = r_e^2\hat{\nu}, \tag{50}$$

$$\omega = r_e^2\hat{\omega}. \tag{51}$$

Using these transformations in equations (18) and (40), we have new expressions of the enthalpy and the rotation law as follows:

$$(1+N)\ln(K\varepsilon^{1/N}+1) + r_e^2\hat{\nu} + \tfrac{1}{2}\ln(1-v^2) - \tfrac{1}{2}A^2(\Omega-\Omega_c)^2 = C, \tag{52}$$

$$A^2(\Omega_c-\Omega) = \frac{v^2}{(1-v^2)(\Omega-r_e^2\hat{\omega})}, \tag{53}$$

where

$$v = (\Omega - r_e^2\hat{\omega})r_e\hat{r}\sin\theta\exp[r_e^2(\hat{\beta}-\hat{\nu})]. \tag{54}$$

Solving directly the equations (52) and (53) at three points P, Q and W simultaneously by the Newton–Raphson method, we can obtain six quantities $\Omega(\mathrm{P})$, $\Omega(\mathrm{Q})$, $\Omega(\mathrm{W})$, Ω_c, r_e and C for given metric potentials $\hat{\nu}$, $\hat{\alpha}$, $\hat{\beta}$ and $\hat{\omega}$. Using these values of Ω_c and r_e, we calculate the distribution of the angular velocity Ω by solving equation (53) again by using the Newton–Raphson method. The obtained distribution of Ω is used to calculate the density distribution ε from equation (52). The point W is determined as the maximum density point using the last value of density distribution ε in the iteration cycle. In this process three conditions (43)–(45) at P, Q and W, respectively, are automatically satisfied.

3.4 OVERRELAXATION TECHNIQUE

In order to accelerate the convergence of iteration, we sometimes use the overrelaxation technique (Varga 1962). Three metric potentials, ρ, γ and ω, are calculated from:

$$u^{(k+1)} = w\hat{u}^{(k+1)} + (1-w)u^{(k)}, \tag{55}$$

where $u^{(k)}$ is the kth iteration value of the metric potentials (u denotes one of ρ, γ, and ω) and $\hat{u}^{(k+1)}$'s are newly computed values from equations (33)–(35) by using the values of $u^{(k)}$'s. The numerical factor w, which is a kind of damping factor, is determined experimentally to appropriately accelerate the convergence of iteration.

3.5 COMPUTATIONAL MESH AND DIFFERENCE SCHEME

Each mesh point is denoted by (μ_i, r_j). Here, μ_i is the ith mesh point in the μ-direction and r_j is the jth mesh point in the r-direction, respectively. In the present paper, we use mainly equal mesh intervals. Then the derivatives that appear in each source term of integration can be evaluated by the following second-order accuracy difference formulae:

$$f_{,\mu} \to [f(\mu_{i+1}, r_j) - f(\mu_{i-1}, r_j)]/(2\Delta\mu), \tag{56}$$

$$f_{,r} \to [f(\mu_i, r_{j+1}) - f(\mu_i, r_{j-1})]/(2\Delta r), \tag{57}$$

$$f_{,\mu\mu} \to [f(\mu_{i+1}, r_j) + f(\mu_{i-1}, r_j) - 2f(\mu_i, r_j)]/(\Delta\mu)^2, \tag{58}$$

$$f_{,r\mu} \to [f(\mu_{i+1}, r_{j+1}) - f(\mu_{i+1}, r_{j-1}) - f(\mu_{i-1}, r_{j+1}) + f(\mu_{i-1}, r_{j-1})]/(4\Delta\mu\Delta r), \tag{59}$$

$$f_{,rr} \to [f(\mu_i, r_{j+1}) + f(\mu_i, r_{j-1}) - 2f(\mu_i, r_j)]/(\Delta r)^2, \tag{60}$$

where Δr is the mesh interval in the r-direction and $\Delta\mu$ is the mesh interval in the μ-direction. We use Simpson's formula for the integrations with respect to μ' and r' in equations (33)–(35). Equation (36) is integrated by the trapezoidal formula.

4 Uniformly rotating polytropes

In the present paper, we report only the results of uniformly rotating polytropes with three different polytropic indices, $N=1/2$, $N=3/2$ and $N=3$. If we adopt a large value of A, the rotation law is approaching a rigid one as one can see from equation (18). Here we use $A\varepsilon_{\max}^{1/2} = 100$ for almost all models. For $N=1/2$, two sequences with $\kappa=0.001$ and $\kappa=1$ have been computed. For $N=3/2$, we have computed five sequences having different values of κ, i.e. $\kappa=0.001$, $\kappa=0.25$, $\kappa=0.5$, $\kappa=0.8$ and $\kappa=1$. For $N=3$, two sequences have been computed for $\kappa=0.001$ and $\kappa=0.6$. Our method has worked successfully even for $\kappa=1$ while Butterworth (1976) failed to obtain solutions when $\kappa>0.25$.

The computational region covers from $r=0$ to $r=r_{\max}=2r_e$ and the number of mesh points is 51×101 ($\mu\times r$). Therefore, the region where matter exists includes radial 51 mesh points on the equator. The metric potentials ρ, γ and ω are expanded up to $P_{18}(\mu)$, $\sin 19\theta$ and $P_{19}^1(\mu)$, in equations (33)–(35), respectively. Then one iteration cycle takes 3.0 s computer time on a Fujitsu M-380R processor. A typical number of iterations until the convergence is 30, therefore, one model needs 90 s computer time. Our code is partly checked by the following four kinds of accuracy test: the comparison with the Newtonian results (James 1964; Hachisu 1986a) indicates that they agree each other quite well (see Table 1). The differences are smaller than 1 per cent. By comparing our solutions of non-rotating homogeneous body with the Schwarzschild's analytical interior solutions, metric potentials such as α and β deviate from those for the Schwarzschild's solutions up to 5 per cent but integrated quantities such as the rest mass, the gravitational mass, and the coordinate radius agree well (within to 2–3 per cent) (see Fig. 2). We have also computed several $N=0$ models for accuracy check. The comparison with Butterworth & Ipser's (1976) results indicates that the integrated physical quantities such as the mass and the angular momentum, and the angular velocity agree with each other very well (within 2 or 3 per cent) (see also Table 1). As for the change of the computational space size in the vacuum region, we will discuss its influence on the accuracy of our results in Section 5.

Table 1. Comparison with other results.

(a) $N=3/2$ and Newtonian limit (models at the critical rotation)

	r_p/r_e	$M\varepsilon_{max}^{1/2}$	ℓ^2	$\Omega/\varepsilon_{max}^{1/2}$
James[a]	0.6151	1.133E-4	2.845E-2	0.5235
Hachisu[b]	0.617	1.13E-4	2.87E-2	0.523
$\kappa = 0.001$	0.61	1.12E-4	2.85E-2	0.524

[a]Taken from James (1964).
[b]Taken from Hachisu (1986a).

(b) $N=0$ and relativistic case

	r_p/r_e	$M\varepsilon_{max}^{1/2}$	ℓ^2	$\Omega/\varepsilon_{max}^{1/2}$	$T/\|W\|$
$\kappa = 0.687$[a]		0.120	0.046	1.3	0.14
$\kappa = 0.687$	0.725	0.120	0.0458	1.28	0.139

[a]Taken from Butterworth & Ipser (1976).

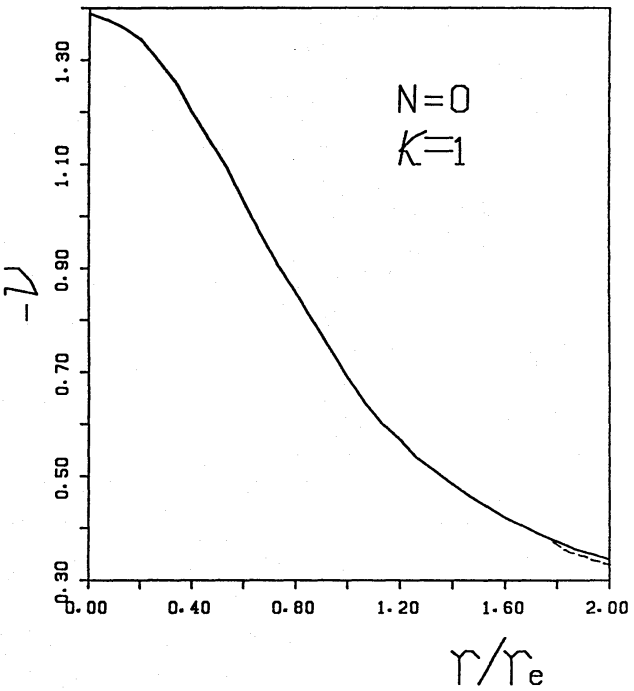

Figure 2. The comparison of our computed models for $N=0$ and $\kappa=1$ with the Schwarzschild's analytical solution (non-rotating case). The ordinate is the absolute value of the gravitational potential ν and the abscissa is the isotropic coordinate radius r. Our result (solid line) agrees well with the analytical solution (dashed line) within to 1 per cent.

4.1 $N=3/2$ POLYTROPES

First we discuss the results of $N=3/2$ case. In Fig. 3 are shown the energy density distributions ε at the critical rotation. There cannot exist equilibrium solutions beyond this critical rotation because mass sheds from the equatorial surface. So we will call it 'mass shedding' to clarify its physical nature. Fig. 3(a) is for the limiting case of strong gravity, i.e. $k=1$. Fig. 3(b) is, on the other hand, for the Newtonian limit, i.e. $\kappa=0.001$. The energy density decreases 10 times from an inner contour to the next outer contour. The figure clearly shows that due to the strong gravity the mass is concentrated into the central region compared with the Newtonian limit.

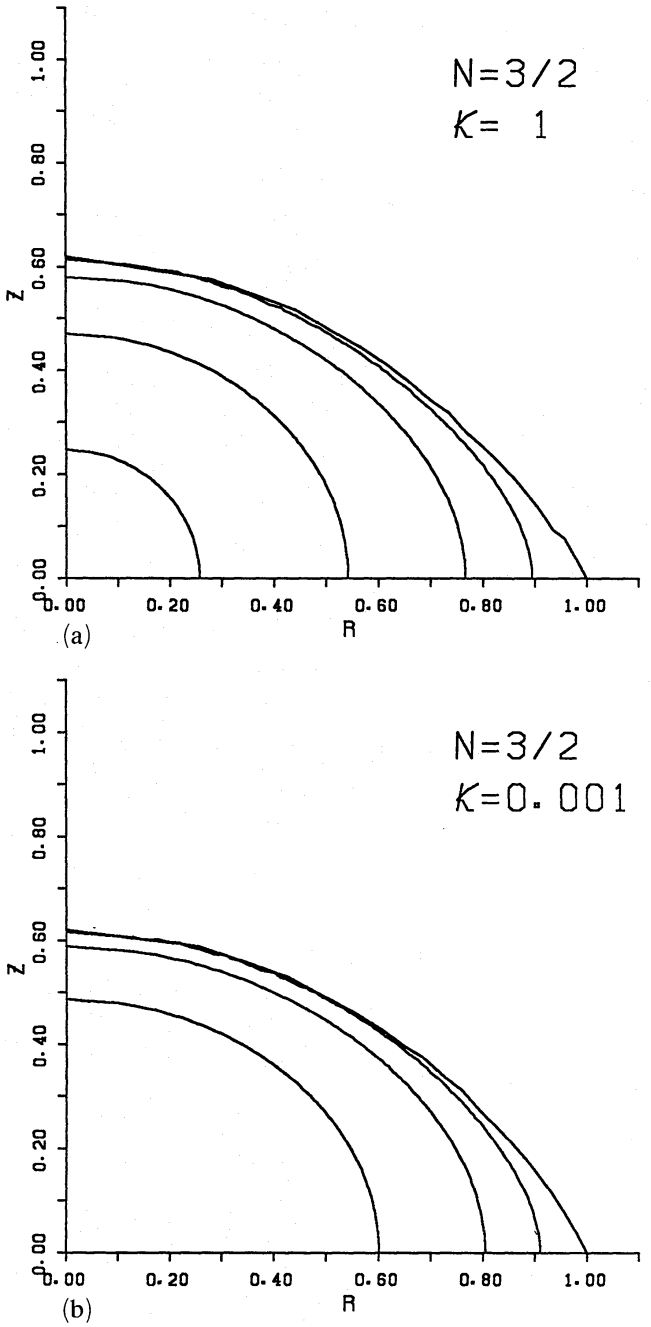

Figure 3. Contours of the energy density ε in the meridional plane for the case of polytropic index $N=3/2$: the critical rotation models for $\kappa=1$ (a) and for $\kappa=0.001$ (b). Energy density changes 10 times between two contours.

The non-dimensional angular velocity $\Omega_c/\varepsilon_{max}^{1/2}$ is plotted against the axis ratio r_p/r_e in Fig. 4. Strictly speaking, the angular velocity is not constant in space but it decreases outward slightly. For a large value of A, however, we can regard that the angular velocity is almost constant in space. Yet note that this very small change in Ω is important for us to calculate Ω_c from the boundary conditions as explained in Section 3. Fig. 4 clearly shows the interesting fact that each sequence is terminated at the almost same axis ratio, i.e. $r_p/r_e=0.60$ regardless of the strength of gravity κ.

The same quantity is plotted against another meaningful physical quantity, i.e. the squared

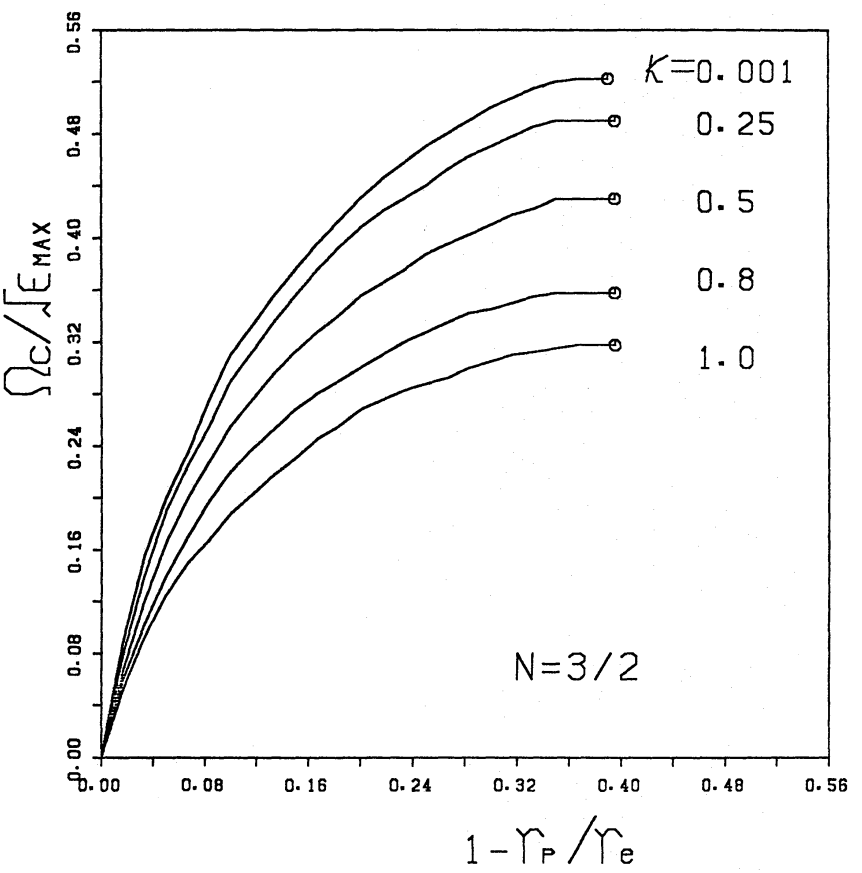

Figure 4. Non-dimensional angular velocity $\Omega_c/\varepsilon_{max}^{1/2}$ is plotted against the coordinate axis ratio r_p/r_c for $N=3/2$. The numbers attached to each line denote the strength of gravity κ. Five sequences correspond to those for $\kappa=1.0$, $\kappa=0.8$, $\kappa=0.5$, $\kappa=0.25$ and $\kappa=0.001$. Each sequence terminates at the critical rotation (open circles).

dimensionless angular momentum l^2, in Fig. 5. The value of l^2 is defined as:

$$l^2 = J^2 \varepsilon_{max}^{1/3} / M_0^{10/3}, \tag{61}$$

where the total angular momentum J and the rest mass M_0 are also defined by:

$$J = 2\pi \int dr \int d\theta\, r^3 \sin^2\theta \frac{(\varepsilon + p)v}{1-v^2} e^{2\alpha+2\beta}, \tag{62}$$

and

$$M_0 = 2\pi \int dr \int d\theta\, r^2 \sin\theta \frac{\varepsilon}{(1+p/\varepsilon)^N} \frac{e^{2\alpha+\beta}}{\sqrt{1-v^2}}. \tag{63}$$

This quantity l^2 is the same as the rotation parameter defined by Bardeen (1971). As shown in Fig. 5, our solutions on the $\kappa=0.001$ sequence are in good agreement with those of the Newtonian case (James 1964; Hachisu 1986a).

The larger the relativistic parameter κ, the smaller the dimensionless angular velocity $\Omega/\varepsilon_{max}^{1/2}$ for the same axis ratio r_p/r_e or for the same squared dimensionless angular momentum l^2. This behaviour can be explained from the fact that due to the strong gravity the mass is concentrated into the central region of the star. The degree of mass concentration is defined by

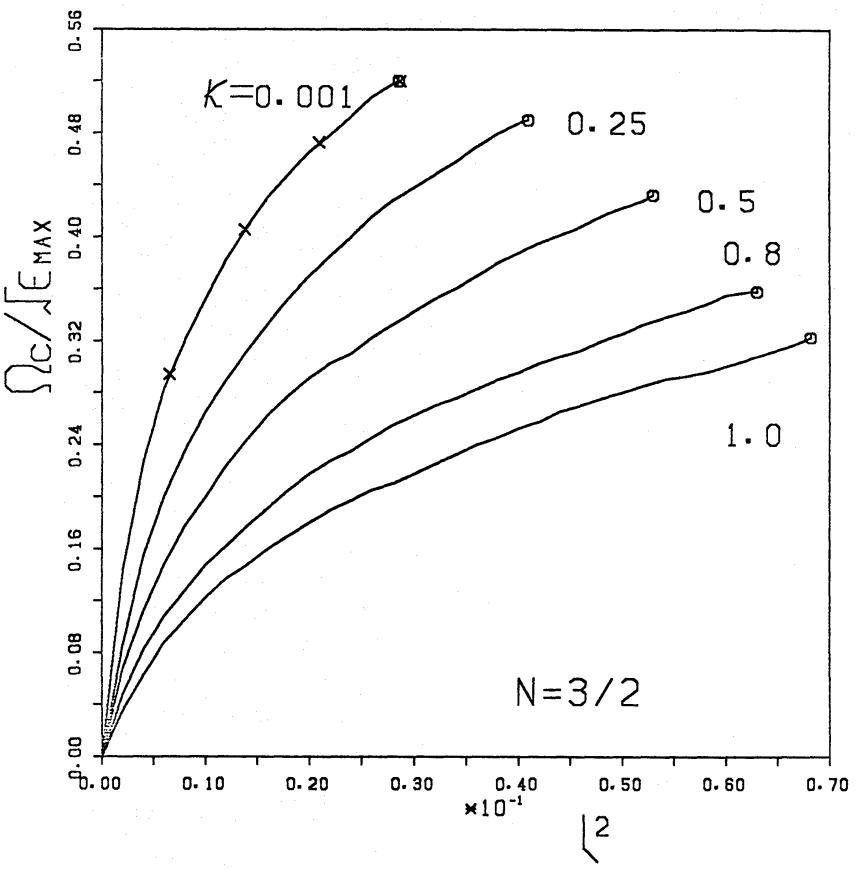

Figure 5. Non-dimensional angular velocity $\Omega_c/\varepsilon_{max}^{1/2}$ is plotted against the dimensionless angular momentum $l^2 = J^2\varepsilon_{max}^{1/3}/M_0^{10/3}$ for $N = 3/2$. Five sequences for $\kappa = 1.0$, $\kappa = 0.8$, $\kappa = 0.5$, $\kappa = 0.25$ and $\kappa = 0.001$ are shown. Symbols have the same meaning as those in Fig. 4. Crosses denote the Newtonian results computed by James (1964) and Hachisu (1986a).

the ratio of the mean energy density to the central energy density, $\bar{\varepsilon}/\varepsilon_{max}$, where $\bar{\varepsilon}$ is defined as follows:

$$\bar{\varepsilon} = M_p/V_p. \tag{64}$$

Here, the proper mass M_p and the proper volume V_p are calculated from:

$$M_p = \int \varepsilon u^t \sqrt{-g} d^3x = 2\pi \int dr \int d\theta r^2 \sin\theta \varepsilon \frac{e^{2\alpha+\beta}}{\sqrt{1-v^2}}, \tag{65}$$

$$V_p = \int u^t \sqrt{-g} d^3x = 2\pi \int dr \int d\theta r^2 \sin\theta \frac{e^{2\alpha+\beta}}{\sqrt{1-v^2}}. \tag{66}$$

Easily seen from Fig. 3, this value of $\bar{\varepsilon}/\varepsilon_{max}$ becomes smaller as the strength of gravity κ increases. Contours of the energy density in the central region hardly deviates from a sphere as seen from Fig. 3(a). The mass contained in the outer region is too small to affect the gravity, therefore, the gravitational force near the equatorial surface can be approximated by that for a spherical model. Introducing the effective gravity G_{eff} to incorporate the effect of general relativity, we have the following expression at the critical rotation:

$$r_e\Omega_{crit}^2 = G_{eff}M/r_e^2, \tag{67}$$

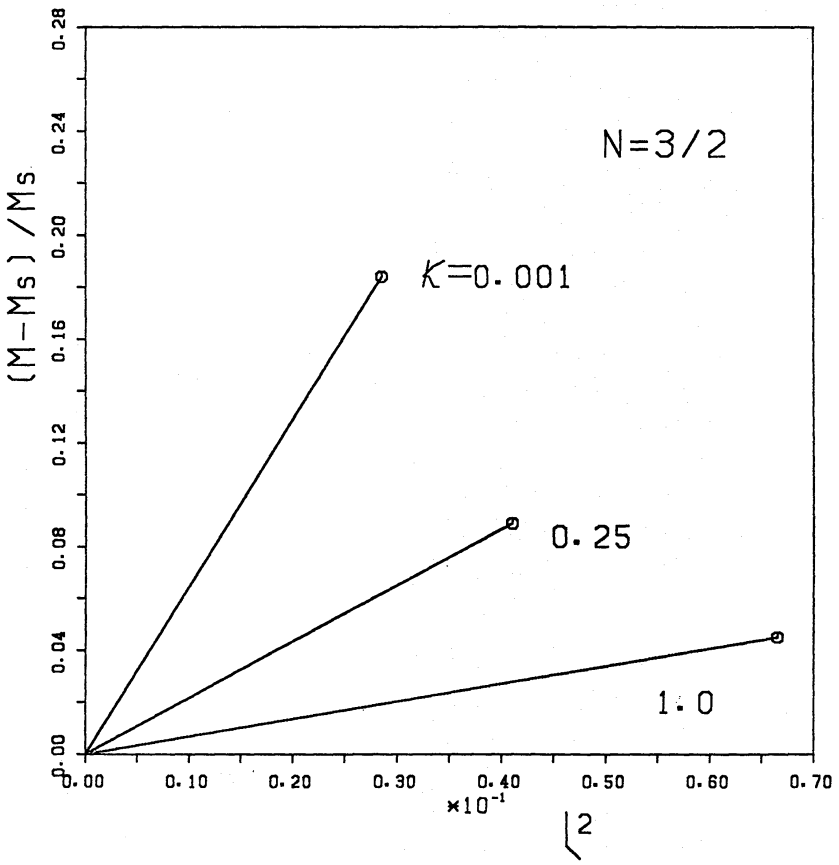

Figure 6. The increase in the gravitational mass $(M-M_s)/M_s$ against the squared dimensionless angular momentum l^2. Here M_s is the gravitational mass of non-rotating spherical model for the same value of κ. The polytropic index is $N=3/2$.

where M is the gravitational mass defined by:

$$M=2\pi\iint dr\,d\theta\,r^2\sin\theta\,e^{2\alpha+\beta}\left[e^{\nu}\left(\frac{(\varepsilon+p)(1+v^2)}{1-v^2}+2p\right)+2r\sin\theta\,\omega e^{\beta}\frac{(\varepsilon+p)v}{1-v^2}\right]. \tag{68}$$

Then $\Omega_{\rm crit}$ is expressed as:

$$\Omega_{\rm crit}/\varepsilon_{\rm max}^{1/2}=[(G_{\rm eff}M/r_{\rm e}^3)/\varepsilon_{\rm max}]^{1/2}\propto(\bar{\varepsilon}/\varepsilon_{\rm max})^{1/2}. \tag{69}$$

It is clear that $\Omega_{\rm crit}/\varepsilon_{\rm max}^{1/2}$ becomes smaller with decreasing $\bar{\varepsilon}/\varepsilon_{\rm max}$.

In Fig. 6, the increase in the gravitational mass is plotted against the squared dimensionless angular momentum l^2. For the Newtonian case, rotation can increase the mass up to 20 per cent. For the case of strong gravity, however, the critical rotation is reached long before the gravitational mass increases substantially. As a result, the increase in the gravitational mass is suppressed to 5 per cent.

In Fig. 7, the ratio of the rotational kinetic energy to the total gravitational energy $T/|W|$ is plotted. Here the rotational energy T and the gravitational energy $|W|$ are defined as:

$$T=\frac{1}{2}\int\Omega\,dJ=\pi\int dr\int d\theta\,r^3\sin^2\theta\frac{(\varepsilon+p)v}{1-v^2}\Omega e^{2\alpha+2\beta}, \tag{70}$$

$$|W|=M_{\rm p}+T-M. \tag{71}$$

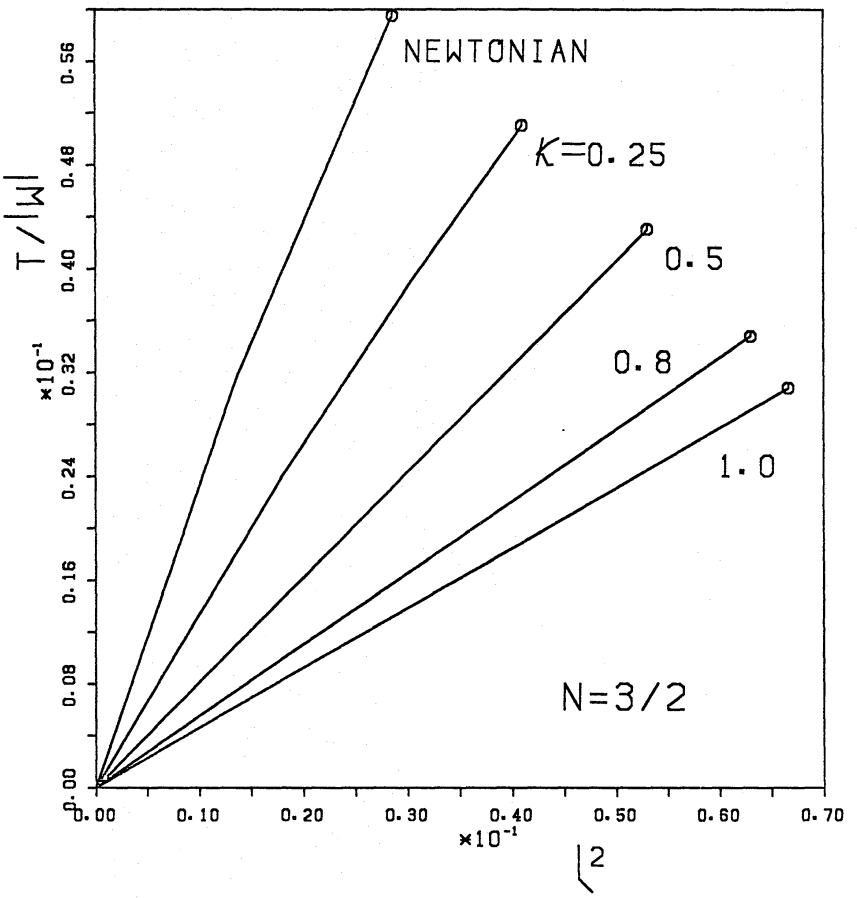

Figure 7. The ratio of the rotational energy to the total gravitational energy $T/|W|$ is plotted against the squared dimensionless angular momentum I^2. The polytropic index is $N=3/2$. The uppermost curve is taken from the Newtonian case computed by Hachisu (1986a).

The value of $T/|W|$ increases up to 0.0308 for $\kappa=1$. For the less strong gravity case of $\kappa=0.25$, it does up to 0.0511. This tendency is the same as the results of Butterworth (1976).

4.2 $N=1/2$ POLYTROPES

Next we disccuss the $N=1/2$ case. Fig. 8 shows the energy density distributions in the meridional plane for two critical rotation models, i.e. $\kappa=1$ and $\kappa=0.001$. As seen in the figure, the mass concentration is not so remarkable as that for $N=3/2$ as mentioned before.

Fig. 9 shows the dimensionless angular velocity $\Omega_c/\varepsilon_{max}^{1/2}$ against the axis ratio r_p/r_e. Fig. 10 also shows $\Omega_c/\varepsilon_{max}^{1/2}$ against the dimensionless angular momentum I^2. As a result of non-significant mass concentration, the difference between the $\kappa=1$ and $\kappa=0.001$ sequences, for the same axis ratio or for the same dimensionless angular momentum, is not so large as compared with the case of $N=3/2$ (see Figs 4 and 5). As seen in Fig. 9, the angular velocity for $\kappa=1$ is always larger than that for $\kappa=0.001$. This is partly because G_{eff} in equation (67) is large for the strong gravity and its effect surmounts the effect of the weak mass concentration. The other reason will be discussed later. The mass shedding occurs earlier (at $r_p/r_e=0.58$) than in the Newtonian case (at $r_p/r_e=0.45$). This tendency is consistent with the results of Butterworth & Ipser's (1976) $N=0$ (constant ε) models.

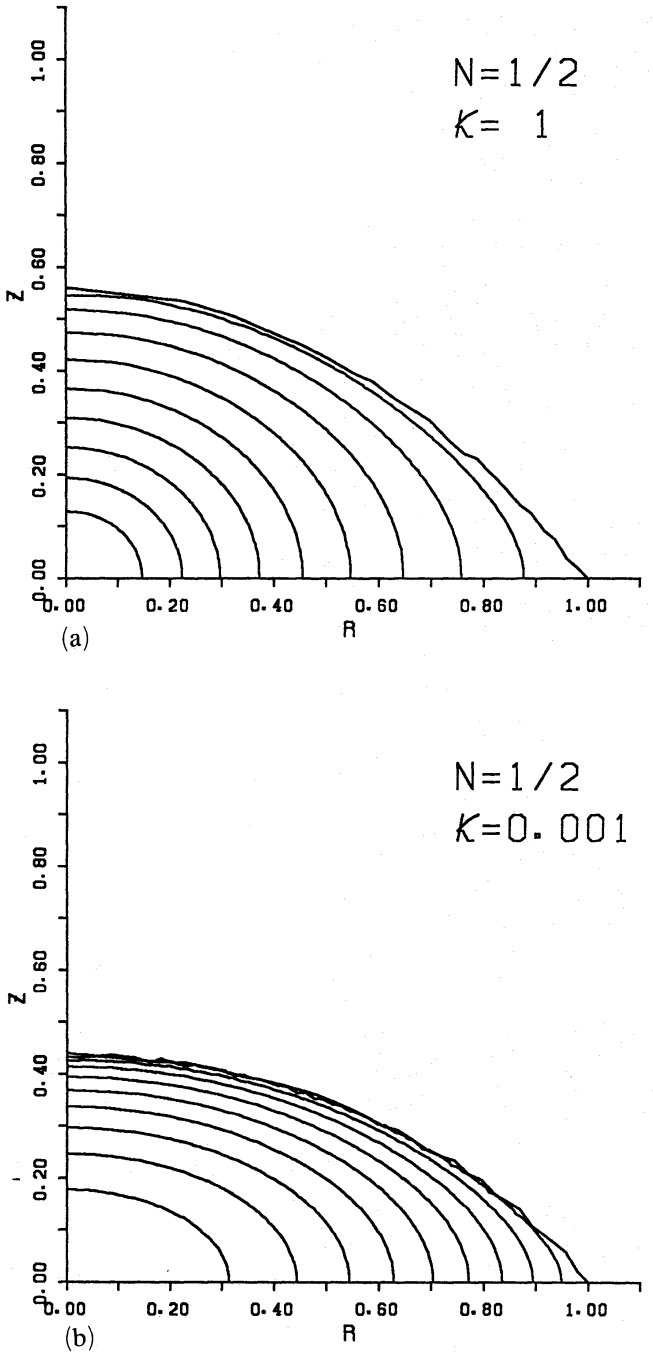

Figure 8. Contours of the energy density ε in the meridional plane for $N=1/2$: the critical rotation models for $\kappa=1$ (a) and for $\kappa=0.001$ (b). Energy density contours are linearly spaced (a tenth of $\varepsilon_{\max}$).

Fig. 11 depicts the dragging of the inertial frame ω/Ω in the equatorial plane. The dragging of the $N=1/2$ model is larger than that of the $N=3/2$ model in the whole region of the star because the gravity near the outer region is rather strong due to the nearly constant energy density of the $N=1/2$ models. For nearly constant ε bodies such as $N=1/2$ models, the dragging of the inertial frame becomes so important in the whole region that the larger angular velocity is needed to attain the same deformation (Miller 1977). Because of its much larger angular velocity, mass sheddings take place at larger axis ratios for the highly relativistic case

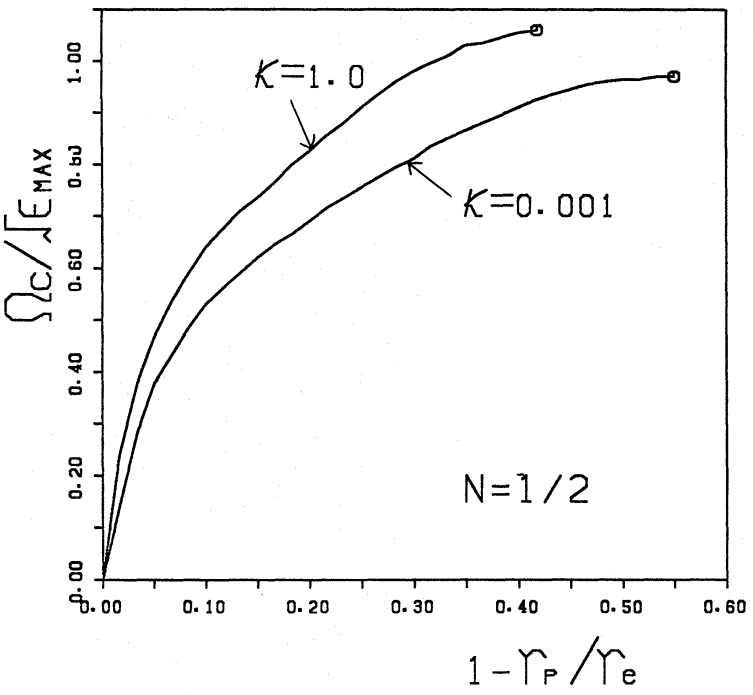

Figure 9. Same as Fig. 4 but for $N=1/2$. Two sequences for $\kappa=0.001$ and $\kappa=1$ are shown.

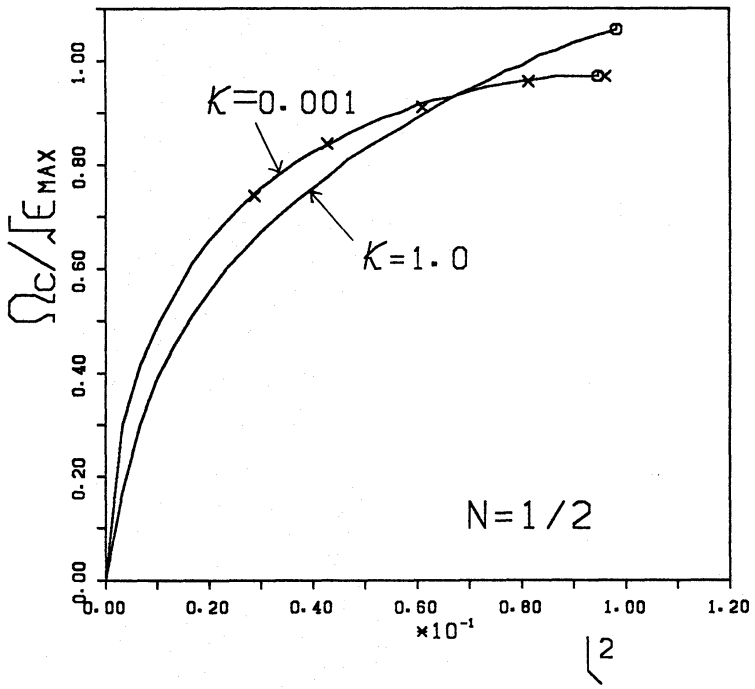

Figure 10. Same as Fig. 5 but for $N=1/2$. Two sequences for $\kappa=0.001$ and $\kappa=1$ are shown. Crosses denote the Newtonian results computed by Hachisu (1986a).

(Fig. 9). This was explained first by Butterworth & Ipser (1976) in detail. The increase of gravitational mass at the mass shedding is suppressed to 21 per cent for $\kappa=1$ while it increases to 90 per cent for the Newtonian case ($\kappa=0.001$). The increase in the gravitational mass is plotted against the dimensionless angular momentum l^2 in Fig. 12.

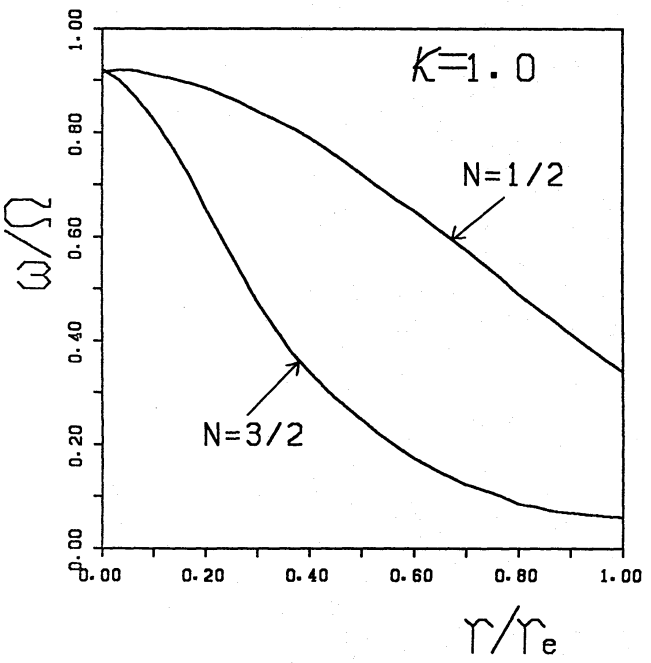

Figure 11. The dragging of the inertial frame ω/Ω in the equatorial plane is plotted against the coordinate radius in units of equatorial radius r_e for two critical rotating models for $N=1/2$ and $N=3/2$ with $\kappa=1$.

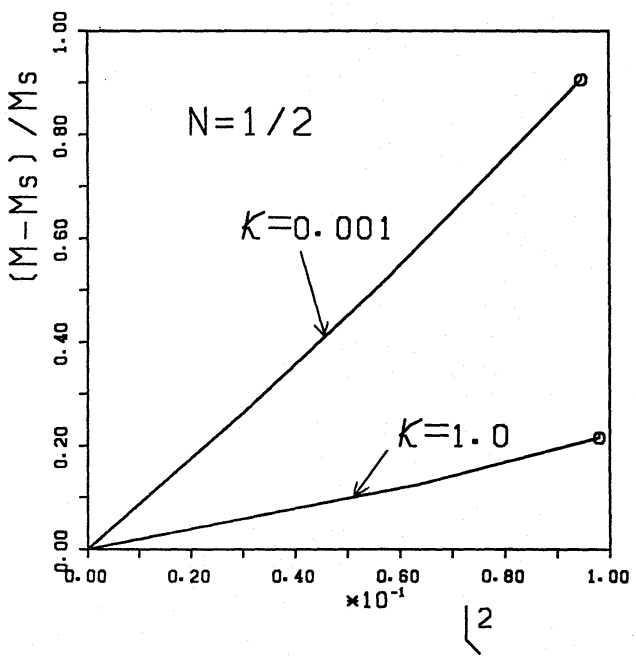

Figure 12. Same as Fig. 6 but for $N=1/2$.

Finally the metric potentials $e^{2\nu}$ and $e^{2\beta}$ in the equatorial plane for the $\kappa=1$ models are drawn against r/r_e in Figs 13 and 14. For comparison the same quantities for $N=3/2$ polytrope are also plotted. The potential $e^{2\beta}$ is related to the proper circumferential radius r_s in the equatorial plane as: $r_s=re^{\beta}$. The rather large difference between two curves of $e^{2\nu}$ for $N=3/2$ is caused by the increase of the equatorial radius r_e when the rotation is increased. However, it is remarkable that the value of $e^{2\beta}$ at the equator is hardly affected by the rotation especially for the $N=1/2$ case.

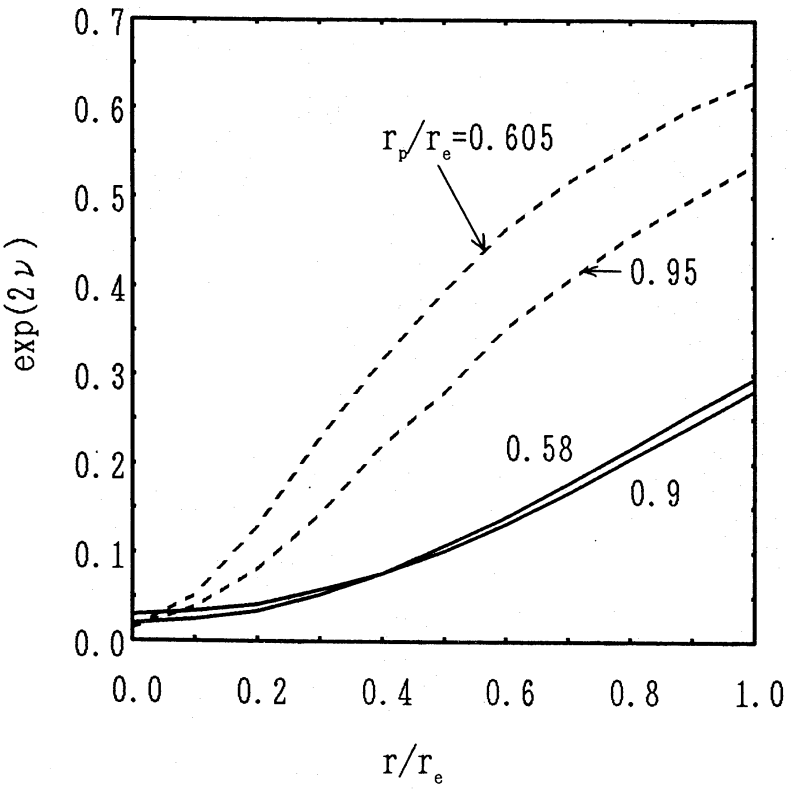

Figure 13. The metric coefficient $e^{2\nu}$ in the equatorial plane is plotted against the radial coordinate in units of the equatorial radius r/r_e. The upper pair of dashed curves represent the models with $N=3/2$ and $\kappa=1$ and the lower pair of solid curves the models with $N=1/2$ and $\kappa=1$.

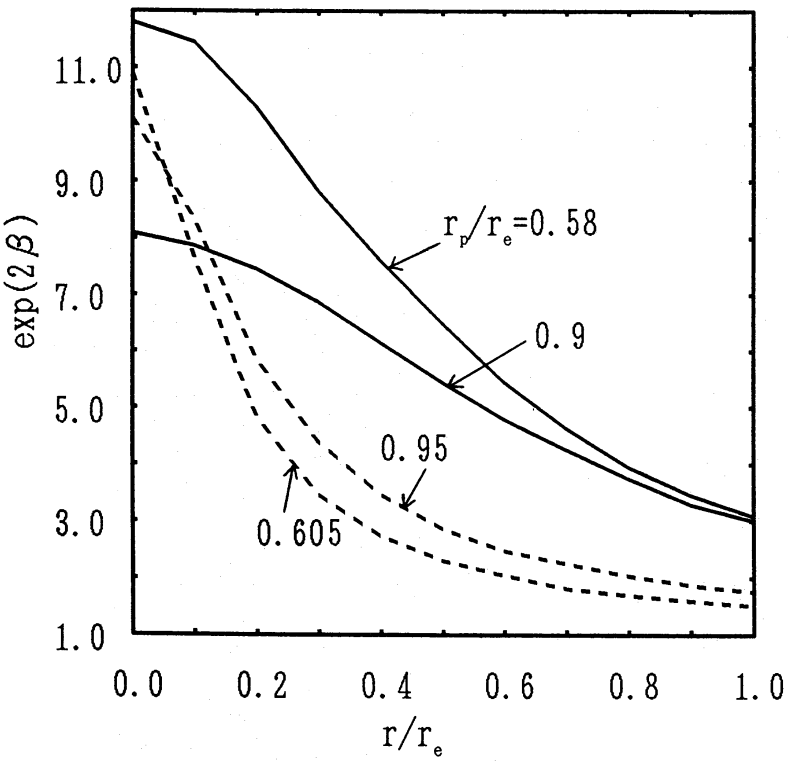

Figure 14. Same as Fig. 13 but for $e^{2\beta}$. The upper pair of solid curves represent the models with $N=1/2$ and $\kappa=1$ and the lower pair of dashed curves the models with $N=3/2$ and $\kappa=1$.

4.3 $N=3$ POLYTROPES

For the case of $N=3$, the mass concentration is significant and a numerical instability prevented us from computing models when $\kappa > 0.6$. So, we computed two sequences for $\kappa = 0.001$ and $\kappa = 0.6$ until the mass shedding occurs. To obtain models with $\kappa = 0.6$, we used $A\varepsilon_{\max}^{1/2} = 1000$ and the following radial coordinate $\hat{R}$:

$$\hat{r} = \exp(a\hat{R}) - 1. \tag{72}$$

The mesh in the $\hat{R}$-coordinate has an equal mesh spacing. The value of a is chosen to be 6.5. Our numerical values of the proper volume V_p can be determined within factor 1.5 because the radial interval between two mesh points is large near the stellar surface as can be seen from equation (72). But the accuracy checks which were made by changing the value of a and by comparing with spherical models (Tooper 1964) show that as for other quantities such as the mass, the angular momentum, the rotational energy, and the angular velocity, the errors are within to 5 per cent (see Table 2).

Table 2. Physical properties of spherical models ($N=3$ and $\kappa=0.4$).

		$M\varepsilon_{max}^{1/2}$	$\lvert W\rvert/M$	$M_0\varepsilon_{max}^{1/2}$	$V_p\varepsilon_{max}^{3/2}$	$\bar{\varepsilon}/\varepsilon_{max}$
Tooper[a]		0.2578	0.3222			
present	a=3.5	0.259	0.319	0.213	1.1E+3	3.2E-4
	a=2.5	0.266	0.302	0.220	1.5E+3	2.3E-4

[a]Taken from Tooper (1964).

Because the mass is extremely concentrated to the central region for the case with $\kappa = 0.6$, the mass shedding occurs at very early stage, i.e. $\Omega_c/\varepsilon_{\max}^{1/2} = 1.46\times10^{-3}$ and $T/|W| = 5.75\times10^{-5}$ in contrast to the Newtonian case for which $\Omega_c/\varepsilon_{\max}^{1/2} = 0.159$ and $T/|W| = 8.94\times10^{-3}$. These values are in qualitative agreement with equation (69) because $\bar{\varepsilon}/\varepsilon_{\max}$ of $\kappa = 0.6$ is 10^{-4} times smaller than that of $\kappa = 0.001$.

In Table 3 we summarize the physical quantities for various sequences having different values of κ and N.

Table 3(a). $N=3/2$ $\kappa=0.25$.

r_p/r_e	$\Omega_c/\varepsilon_{max}^{1/2}$	ℓ^2	$M_0\varepsilon_{max}^{1/2}$	$r_e\varepsilon_{max}^{1/2}$	$M\varepsilon_{max}^{1/2}$	$M_p\varepsilon_{max}^{1/2}$	$T/\lvert W\rvert$	v_e^a
1.00	0.0	0.0	0.119	0.458	0.112	0.141	0.0	0.0
0.95	0.194	4.96E-3	0.120	0.473	0.113	0.142	6.83E-3	0.128
0.90	0.292	1.18E-2	0.122	0.486	0.115	0.144	1.60E-2	0.200
0.85	0.354	1.80E-2	0.123	0.504	0.117	0.146	2.40E-2	0.249
0.80	0.409	2.52E-2	0.125	0.522	0.118	0.148	3.29E-2	0.299
0.75	0.445	3.10E-2	0.127	0.547	0.120	0.150	3.98E-2	0.338
0.70	0.472	3.63E-2	0.128	0.577	0.121	0.152	4.60E-2	0.377
0.65	0.487	3.95E-2	0.129	0.616	0.122	0.153	4.96E-2	0.408
*0.605	0.492	4.09E-2	0.130	0.660	0.122	0.153	5.11E-2	0.446

[a]The proper velocity at the equatorial surface.
*The critical rotation.
The value of $\bar{\varepsilon}/\varepsilon_{\max}$ for the spherical model is 0.135.

Table 3(b). $N=3/2$ $\kappa=0.5$.

r_p/r_e	$\Omega_c/\varepsilon_{max}^{1/2}$	ℓ^2	$M_0\varepsilon_{max}^{1/2}$	$r_e\varepsilon_{max}^{1/2}$	$M\varepsilon_{max}^{1/2}$	$M_p\varepsilon_{max}^{1/2}$	$T/\|W\|$	v_e
1.00	0.0	0.0	0.170	0.540	0.167	0.229	0.0	0.0
0.95	0.172	6.91E-3	0.172	0.557	0.168	0.230	6.06E-3	0.150
0.90	0.259	1.62E-2	0.173	0.572	0.170	0.232	1.40E-2	0.228
0.85	0.313	2.45E-2	0.175	0.593	0.172	0.234	2.09E-2	0.283
0.80	0.361	3.37E-2	0.177	0.615	0.173	0.237	2.84E-2	0.339
0.75	0.391	4.09E-2	0.179	0.645	0.175	0.238	3.41E-2	0.381
0.70	0.415	4.73E-2	0.180	0.681	0.176	0.240	3.91E-2	0.428
0.65	0.427	5.10E-2	0.181	0.727	0.177	0.241	4.19E-2	0.461
*0.605	0.431	5.25E-2	0.181	0.779	0.178	0.241	4.30E-2	0.487

The value of $\bar{\varepsilon}/\varepsilon_{max}$ for the spherical model is 0.102.

Table 3(c). $N=3/2$ $\kappa=0.8$.

r_p/r_e	$\Omega_c/\varepsilon_{max}^{1/2}$	ℓ^2	$M_0\varepsilon_{max}^{1/2}$	$r_e\varepsilon_{max}^{1/2}$	$M\varepsilon_{max}^{1/2}$	$M_p\varepsilon_{max}^{1/2}$	$T/\|W\|$	v_e
1.00	0.0	0.0	0.201	0.644	0.207	0.299	0.0	0.0
0.95	0.145	8.72E-3	0.202	0.665	0.208	0.300	5.10E-3	0.152
0.90	0.218	2.03E-2	0.204	0.685	0.210	0.302	1.18E-2	0.235
0.85	0.263	3.04E-2	0.205	0.710	0.212	0.304	1.75E-2	0.291
0.80	0.303	4.15E-2	0.207	0.738	0.214	0.306	2.36E-2	0.347
0.75	0.328	5.00E-2	0.209	0.775	0.215	0.308	2.82E-2	0.390
0.70	0.347	5.73E-2	0.210	0.819	0.217	0.310	3.21E-2	0.436
0.65	0.356	6.15E-2	0.211	0.876	0.218	0.311	3.42E-2	0.469
*0.607	0.360	6.31E-2	0.211	0.935	0.218	0.311	3.50E-2	0.495

The value of $\bar{\varepsilon}/\varepsilon_{max}$ for the spherical model is 0.0730.

Table 3(d). $N=3/2$ $\kappa=1.0$.

r_p/r_e	$\Omega_c/\varepsilon_{max}^{1/2}$	ℓ^2	$M_0\varepsilon_{max}^{1/2}$	$r_e\varepsilon_{max}^{1/2}$	$M\varepsilon_{max}^{1/2}$	$M_p\varepsilon_{max}^{1/2}$	$T/\|W\|$	v_e
1.00	0.0	0.0	0.215	0.724	0.229	0.336	0.0	0.0
0.95	0.159	1.48E-2	0.217	0.749	0.231	0.339	7.05E-3	0.189
0.90	0.220	2.91E-2	0.219	0.780	0.233	0.341	1.37E-2	0.269
0.85	0.248	3.80E-2	0.220	0.805	0.235	0.342	1.78E-2	0.312
0.80	0.271	4.62E-2	0.222	0.834	0.236	0.343	2.16E-2	0.349
0.75	0.295	5.66E-2	0.223	0.889	0.238	0.345	2.63E-2	0.399
0.70	0.310	6.38E-2	0.224	0.960	0.239	0.346	2.95E-2	0.448
0.65	0.313	6.62E-2	0.225	1.019	0.240	0.346	3.06E-2	0.473
*0.605	0.313	6.64E-2	0.225	1.091	0.240	0.345	3.08E-2	0.481

The value of $\bar{\varepsilon}/\varepsilon_{max}$ for the spherical model is 0.0585.

Table 3(e). $N=1/2$ $\kappa=1.0$.

r_p/r_e	$\Omega_c/\varepsilon_{max}^{1/2}$	ℓ^2	$M_0\varepsilon_{max}^{1/2}$	$r_e\varepsilon_{max}^{1/2}$	$M\varepsilon_{max}^{1/2}$	$M_p\varepsilon_{max}^{1/2}$	$T/\|W\|$	v_e
1.00	0.0	0.0	0.187	0.251	0.147	0.214	0.0	0.0
0.95	0.461	1.38E-2	0.190	0.251	0.151	0.218	2.46E-2	0.222
0.90	0.642	2.81E-2	0.194	0.252	0.155	0.222	4.90E-2	0.317
0.85	0.735	3.81E-2	0.197	0.253	0.158	0.225	6.56E-2	0.369
0.80	0.813	4.85E-2	0.200	0.255	0.161	0.229	8.23E-2	0.424
0.75	0.910	6.41E-2	0.205	0.259	0.166	0.235	1.07E-1	0.482
0.70	0.984	7.92E-2	0.211	0.265	0.171	0.241	1.29E-1	0.543
0.65	1.020	8.80E-2	0.215	0.272	0.175	0.245	1.42E-1	0.583
0.60	1.046	9.49E-2	0.218	0.283	0.177	0.248	1.53E-1	0.621
*0.58	1.058	9.79E-2	0.219	0.299	0.179	0.249	1.57E-1	0.658

The value of $\bar{\varepsilon}/\varepsilon_{max}$ for the spherical model is 0.443.

Table 3(f). $N=3$ $\kappa=0.6$.

r_p/r_e	$\Omega_c/\varepsilon_{max}^{1/2}$	ℓ^2	$M_0\varepsilon_{max}^{1/2}$	$M\varepsilon_{max}^{1/2}$	$M_p\varepsilon_{max}^{1/2}$	$T/\|W\|$
1.00	0.0	0.0	0.393	0.477	0.618	0.0
0.90	1.16E-3	1.56E-3	0.393	0.478	0.619	3.44E-5
0.80	1.40E-3	2.40E-3	0.395	0.479	0.620	5.17E-5
*0.70	1.46E-3	2.69E-3	0.396	0.481	0.622	5.75E-5

5 Discussion

In our numerical models, ergoregions where any observer must rotate relative to infinity do not appear. Therefore our models are free from the relativistic instability which is accompanied by the existence of the ergoregions (Butterworth & Isper 1976; Friedman 1978).

Our numerical technique is the so-called self-consistent field method and is almost the same as that adopted by Bonazzola & Schneider (1974). But our method is different from theirs in the following points. First, we fix the two edges of star in our computational space during the iteration cycles. Second, the maximum density is also specified during the iterations. These two conditions can be regarded as the boundary conditions for the matter. Our temporary solutions always satisfy these conditions exactly during the iterations. This is the origin of the robustness of our numerical method.

Third, in Bonazzola & Schneider's treatment, the sum of the two metric potentials $\psi=\alpha+\nu$ is used in an integral form as:

$$\psi=\frac{1}{2\pi}\int_0^{\infty}dr'\int_0^{2\pi}d\theta'\,r'S_{\psi}(r',\theta')\log|\mathbf{r}-\mathbf{r}'|, \tag{73}$$

where

$$S_{\psi}(r,\theta)=8\pi e^{2\alpha}(v^2\varepsilon+p)/(1-v^2)-\nu_{,r}^2-(1/r^2)\nu_{,\theta}^2+\tfrac{3}{4}r^2\sin^2\theta e^{2(\beta-\nu)}[\omega_{,r}^2+(1/r^2)\omega_{,\theta}^2]. \tag{74}$$

If the quantity $S_{\psi}(r,\theta)$ satisfy the following virial theorem (Bonazzola 1973):

$$\int_0^{r}dr\int_0^{2\pi}d\theta\,r\left[8\pi e^{2\alpha}\frac{(v^2\varepsilon+p)}{1-v^2}-\nu_{,r}^2-\frac{1}{r^2}\nu_{,\theta}^2+\frac{3}{4}r^2\sin^2\theta e^{2(\beta-\nu)}\left(\omega_{,r}^2+\frac{1}{r^2}\omega_{,\theta}^2\right)\right]=0+O(1/r), \tag{75}$$

the asymptotic condition $\psi\sim O(1/r)$ for $r\to\infty$ is satisfied. However, during the iteration procedure, it is not guaranteed that the virial theorem holds for the temporary metric potentials if we use equation (73) to calculate $\alpha(=\psi-\nu)$ instead of equation (36). This means that the converged values do not necessarily satisfy the asymptotic condition unless equation (75) is involved in the iteration procedure. Our treatment is free from this difficulty.

As seen from equations (21), (24) and (27), we must cover the whole space ranging from the coordinate centre to the infinity but, in actual computation, we are forced to integrate up to a certain finite radius from the centre. In most cases we have covered twice the larger region than the equatorial radius. For the case of $N=3/2$ and at the critical rotation, reducing the computational region to 1.2 times the equatorial radius, we find that the surface equatorial radius varies only within to 2–3 per cent and the changes of other quantities such as the mass, the angular velocity, and the angular momentum are rather smaller than this change.

Our method can be directly used for obtaining differentially rotating spheroidal configurations and ring configurations, and applicable even to heavy accretion discs around a neutron star or a black hole. We will discuss these subjects in subsequent papers.

Acknowledgments

One of the authors (HK) would like to thank Professor Yoji Osaki for continuous encouragements. IH thanks Joel E. Tohline for hospitality at LSU. The numerical computation were carried out on a Fujitsu M-380R at the Tokyo Astronomical Observatory and partly on an M-380 at the Institute for Space and Astronautical Science. This research was supported in part by the Grant-in-Aid for Scientific Research (62540183, 63540190) of the Japanese Ministry of Education, Science, and Culture and also by the United States National Science Foundation grant AST-8701503.

References

Bardeen, J. M., 1970. *Astrophys. J.*, **162,** 71.
Bardeen, J. M., 1971. *Astrophys. J.*, **167,** 425.
Bonazzola, S., 1973. *Astrophys. J.*, **182,** 335.
Bonazzola, S. & Schneider, J., 1974. *Astrophys. J.*, **191,** 273.
Butterworth, E. M., 1976. *Astrophys. J.*, **204,** 561.
Butterworth, E. M. & Ipser, J. R., 1975. *Astrophys. J.*, **200,** L103.
Butterworth, E. M. & Ipser, J. R., 1976. *Astrophys. J.*, **204,** 200.
Chandrasekhar, S., 1969. *Ellipsoidal Figures of Equilibrium,* Yale University Press, New Haven.
Eriguchi, Y., 1978. *Publs astr. Soc. Japan,* **30,** 507.
Eriguchi, Y., 1980. *Prog. theor. Phys., Kyoto,* **64,** 2009.
Eriguchi, Y. & Müller, E., 1985. *Astr. Astrophys.*, **146,** 260.
Friedman, J. L., 1978. *Communs Math. Phys.*, **63,** 243.
Friedman, J. L., Ipser, J. R. & Parker, L., 1986. *Astrophys. J.*, **304,** 115.
Hachisu, I., 1986a. *Astrophys. J. Suppl.*, **61,** 479.
Hachisu, I., 1986b. *Astrophys. J. Suppl.*, **62,** 461.
Hachisu, I., Eriguchi, Y. & Nomoto, K., 1986a. *Astrophys. J.*, **308,** 161.
Hachisu, I., Eriguchi, Y. & Nomoto, K., 1986b. *Astrophys. J.*, **311,** 214.
Hawking, S. W. & Ellis, G. F. R., 1973. *The Large Scale Structure of Spacetime,* Cambridge University Press.
James, R. A., 1964. *Astrophys. J.*, **140,** 552.
Miller, J. C., 1977. *Mon. Not. R. astr. Soc.*, **179,** 483.
Ostriker, J. P. & Mark, J. W.-K., 1968. *Astrophys. J.*, **151,** 1075.
Stoeckly, R., 1965. *Astrophys. J.*, **142,** 208.
Tooper, R. F., 1964. *Astrophys. J.*, **140,** 434.
Varga, R. S., 1962. *Matrix Iterative Analysis,* Prentice-Hall, Englewood Cliffs, NJ.
Wilson, J. R., 1972. *Astrophys. J.*, **176,** 195.
Wilson, J. R., 1973. *Phys. Rev. Lett.*, **30,** 1082.